5
CAVITATION

5.1 INTRODUCTION

Cavitation occurs in flowing liquid systems when the pressure falls sufficiently low in some region of the flow so that vapor bubbles are formed. Reynolds (1873) was among the first to attempt to explain the unusual behavior of ship propellers at higher rotational speeds by focusing on the possibility of the entrainment of air into the wakes of the propellor blades, a phenomenon we now term *ventilation.* He does not, however, seem to have envisaged the possibility of vapor-filled wakes, and it was left to Parsons (1906) to recognize the role played by vaporization. He also conducted the first experiments on *cavitation* and the phenomenon has been a subject of intensive research ever since because of the adverse effects it has on performance, because of the noise it creates and, most surprisingly, the damage it can do to nearby solid surfaces. In this chapter we examine various features and characteristics of cavitating flows.

5.2 KEY FEATURES OF BUBBLE CAVITATION

5.2.1 Cavitation inception

It is conventional to characterize how close the pressure in the liquid flow is to the vapor pressure (and therefore the potential for cavitation) by means of the *cavitation number*, σ, defined by

$$\sigma = \frac{p_\infty - p_V(T_\infty)}{\frac{1}{2}\rho_L U_\infty^2} \tag{5.1}$$

where U_∞, p_∞ and T_∞ are respectively a reference velocity, pressure and temperature in the flow (usually upstream quantities), ρ_L is the liquid density and $p_V(T_\infty)$ is the saturated vapor pressure. In a particular flow as σ is

reduced, cavitation will first be observed to occur at some particular value of σ called the incipient cavitation number and denoted by σ_i. Further reduction in σ below σ_i would cause an increase in the number and size of the vapor bubbles.

Suppose that prior to cavitation inception, the magnitude of the lowest pressure in the single phase flow is given by the minimum value of the coefficient of pressure, C_{pmin}. Note that C_{pmin} is a *negative* number and that its value could be estimated from either experiments on or calculations of the single phase flow. Then, *if cavitation inception were to occur when the minimum pressure reaches the vapor pressure* it would follow that the value of the critical inception number, σ_i, would be simply given by

$$\sigma_i = -C_{pmin} \tag{5.2}$$

Unfortunately, many factors can cause the actual values of σ_i to depart radically from $-C_{pmin}$ and much research has been conducted to explore these departures because of the importance of determining σ_i accurately. Among the important factors are

1. the ability of the liquid to sustain a tension so that bubbles do not grow to observable size until the pressure falls a finite amount below the vapor pressure. The magnitude of this tension is a function of the contamination of the liquid and, in particular, the size and properties of the microscopic bubbles (*cavitation nuclei*) that grow to produce the observable vapor bubbles (see, for example, Billet 1985).
2. the fact the cavitation nuclei require a finite residence time in which to grow to observable size.
3. the fact that measurements or calculations usually yield a minimum coefficient of pressure that is a time-averaged value. On the other hand many of the flows with which one must deal in practice are turbulent and, therefore, nuclei in the middle of turbulent eddies may experience pressures below the vapor pressure even when the mean pressure is greater than the vapor pressure.

Moreover, since water tunnel experiments designed to measure σ_i are often carried out at considerably reduced scale, it is also critical to know how to scale up these effects to accurately anticipate inception at the full scale. A detailed examination of these effects is beyond the scope of this text and the reader is referred to Knapp, Daily and Hammitt (1970), Acosta and Parkin (1975), Arakeri (1979) and Brennen (1995) for further discussion.

The stability phenomenon described in section 4.2.5 has important consequences in many cavitating flows. To recognize this, one must visualize a spectrum of sizes of cavitation nuclei being convected into a region of low

pressure within the flow. Then the p_∞ in equations 4.37 and 4.43 will be the local pressure in the liquid surrounding the bubble, and p_∞ must be less than p_V for explosive cavitation growth to occur. It is clear from the above analysis that all of the nuclei whose size, R, is greater than some critical value will become unstable, grow explosively, and cavitate, whereas those nuclei smaller than that critical size will react passively and will therefore not become visible to the eye. Though the actual response of the bubble is dynamic and p_∞ is changing continuously, we can nevertheless anticipate that the critical nuclei size will be given approximately by $4S/3(p_V - p_\infty)^*$ where $(p_V - p_\infty)^*$ is some representative measure of the tension in the low-pressure region. Note that the lower the pressure level, p_∞, the smaller the critical size and the larger the number of nuclei that are activated. This accounts for the increase in the number of bubbles observed in a cavitating flow as the pressure is reduced.

It will be useful to develop an estimate of the maximum size to which a cavitation bubble grows during its trajectory through a region where the pressure is below the vapor pressure. In a typical external flow around a body characterized by the dimension, ℓ, it follows from equation 4.31 that the rate of growth is roughly given by

$$\frac{dR}{dt} = U_\infty(-\sigma - C_{pmin})^{\frac{1}{2}} \tag{5.3}$$

It should be emphasized that equation 4.31 implies explosive growth of the bubble, in which the volume displacement is increasing like t^3.

To obtain an estimate of the maximum size to which the cavitation bubble grows, R_m, a measure of the time it spends below vapor pressure is needed. Assuming that the pressure distribution near the minimum pressure point is roughly parabolic (see Brennen 1995) the length of the region below vapor pressure will be proportional to $\ell(-\sigma - C_{pmin})^{\frac{1}{2}}$ and therefore the time spent in that region will be the same quantity divided by U_∞. The result is that an estimate of maximum size, R_m, is

$$R_m \approx 2\ell(-\sigma - C_{pmin}) \tag{5.4}$$

where the factor 2 comes from the more detailed analysis of Brennen (1995). Note that, whatever their initial size, all activated nuclei grow to roughly the same maximum size because both the asymptotic growth rate (equation 4.31) and the time available for growth are essentially independent of the size of the original nucleus. For this reason all of the bubbles in a bubbly cavitating flow grow to roughly the same size (Brennen 1995).

5.2.2 Cavitation bubble collapse

We now examine in more detail the mechanics of cavitation bubble collapse. As demonstrated in a preliminary way in section 4.2.4, vapor or cavitation bubble collapse in the absence of thermal effects can lead to very large interface velocities and very high localized pressures. This violence has important technological consequences for it can damage nearby solid surfaces in critical ways. In this and the following few sections, we briefly review the fundamental processes associated with the phenomena of cavitation bubble collapse. For further details, the reader is referred to more specialized texts such as Knapp *et al.* (1975), Young (1989) or Brennen (1995).

The analysis of section 4.2.4 allowed approximate evaluation of the magnitudes of the velocities, pressures, and temperatures generated by cavitation bubble collapse (equations 4.32, 4.34, 4.35) under a number of assumptions including that the bubble remains spherical. Though it will be shown in section 5.2.3 that collapsing bubbles do not remain spherical, the spherical analysis provides a useful starting point. When a cavitation bubble grows from a small nucleus to many times its original size, the collapse will begin at a maximum radius, R_m, with a partial pressure of gas, p_{Gm}, that is very small indeed. In a typical cavitating flow R_m is of the order of 100 times the original nuclei size, R_o. Consequently, if the original partial pressure of gas in the nucleus was about 1 *bar* the value of p_{Gm} at the start of collapse would be about 10^{-6} *bar*. If the typical pressure depression in the flow yields a value for $(p^*_\infty - p_\infty(0))$ of, say, 0.1 *bar* it would follow from equation 4.34 that the maximum pressure generated would be about 10^{10} *bar* and the maximum temperature would be 4×10^4 times the ambient temperature! Many factors, including the diffusion of gas from the liquid into the bubble and the effect of liquid compressibility, mitigate this result. Nevertheless, the calculation illustrates the potential for the generation of high pressures and temperatures during collapse and the potential for the generation of shock waves and noise.

Early work on collapse by Herring (1941), Gilmore (1952) and others focused on the inclusion of liquid compressibility in order to learn more about the production of shock waves in the liquid generated by bubble collapse. Modifications to the Rayleigh-Plesset equation that would allow for liquid compressibility were developed and these are reviewed by Prosperetti and Lezzi (1986). A commonly used variant is that proposed by Keller and Kolodner (1956); neglecting thermal, viscous, and surface tension effects this

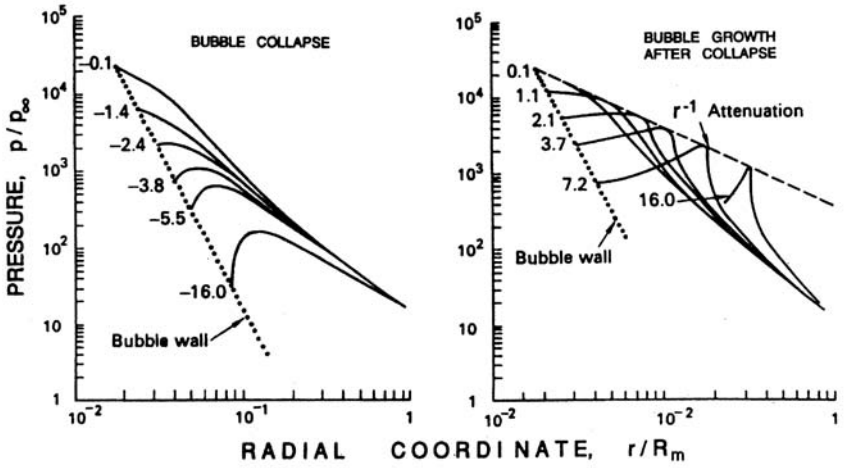

Figure 5.1. Typical results of Hickling and Plesset (1964) for the pressure distributions in the liquid before collapse (left) and after collapse (right) (without viscosity or surface tension). The parameters are $p_\infty = 1$ *bar*, $\gamma = 1.4$, and the initial pressure in the bubble was 10^{-3} *bar*. The values attached to each curve are proportional to the time before or after the minimum size.

is:

$$\left(1 - \frac{1}{c_L}\frac{dR}{dt}\right) R\frac{d^2R}{dt^2} + \frac{3}{2}\left(1 - \frac{1}{3c_L}\frac{dR}{dt}\right)\left(\frac{dR}{dt}\right)^2$$
$$= \left(1 + \frac{1}{c_L}\frac{dR}{dt}\right)\frac{1}{\rho_L}\left\{p_B - p_\infty - p_c(t + R/c_L)\right\} + \frac{R}{\rho_L c_L}\frac{dp_B}{dt} \qquad (5.5)$$

where c_L is the speed of sound in the liquid and $p_c(t)$ denotes the variable part of the pressure in the liquid at the location of the bubble center in the absence of the bubble.

However, as long as there is some non-condensable gas present in the bubble to decelerate the collapse, the primary importance of liquid compressibility is not the effect it has on the bubble dynamics (which is slight) but the role it plays in the formation of shock waves during the rebounding phase that follows collapse. Hickling and Plesset (1964) were the first to make use of numerical solutions of the compressible flow equations to explore the formation of pressure waves or shocks during the rebound phase. Figure 5.1 presents an example of their results for the pressure distributions in the liquid before (left) and after (right) the moment of minimum size. The graph on the right clearly shows the propagation of a pressure pulse or shock away from the bubble following the minimum size. As indicated

in that figure, Hickling and Plesset concluded that the pressure pulse exhibits approximately geometric attenuation (like r^{-1}) as it propagates away from the bubble. Other numerical calculations have since been carried out by Ivany and Hammitt (1965), Tomita and Shima (1977), and Fujikawa and Akamatsu (1980), among others.

Even if thermal effects are negligible for most of the collapse phase, they play a very important role in the final stage of collapse when the bubble contents are highly compressed by the inertia of the in-rushing liquid. The pressures and temperatures that are predicted to occur in the gas within the bubble during spherical collapse are very high indeed. Since the elapsed times are so small (of the order of microseconds), it would seem a reasonable approximation to assume that the noncondensable gas in the bubble behaves adiabatically. Typical of the adiabatic calculations is the work of Tomita and Shima (1977) who obtained maximum gas temperatures as high as $8800°K$ in the bubble center. But, despite the small elapsed times, Hickling (1963) demonstrated that heat transfer between the liquid and the gas is important because of the extremely high temperature gradients and the short distances involved. In later calculations Fujikawa and Akamatsu (1980) included heat transfer and, for a case similar to that of Tomita and Shima, found lower maximum temperatures and pressures of the order of $6700°K$ and 848 *bar* respectively at the bubble center. These temperatures and pressures only exist for a fraction of a microsecond.

All of these analyses assume spherical symmetry. We will now focus attention on the stability of shape of a collapsing bubble before continuing discussion of the origins of cavitation damage.

5.2.3 Shape distortion during bubble collapse

Like any other accelerating liquid/gas interface, the surface of a bubble is susceptible to Rayleigh-Taylor instability, and is potentially unstable when the direction of the acceleration is from the less dense gas toward the denser liquid. Of course, the spherical geometry causes some minor quantitative departures from the behavior of a plane interface; these differences were explored by Birkhoff (1954) and Plesset and Mitchell (1956) who first analysed the Rayleigh-Taylor instability of bubbles. As expected a bubble is most unstable to non-spherical perturbations when it experiences the largest, positive values of d^2R/dt^2. During the growth and collapse cycle of a cavitation bubble, there is a brief and weakly unstable period during the initial phase of growth that can cause some minor roughening of the bubble surface (Reynolds and Berthoud 1981). But, much more important, is the rebound

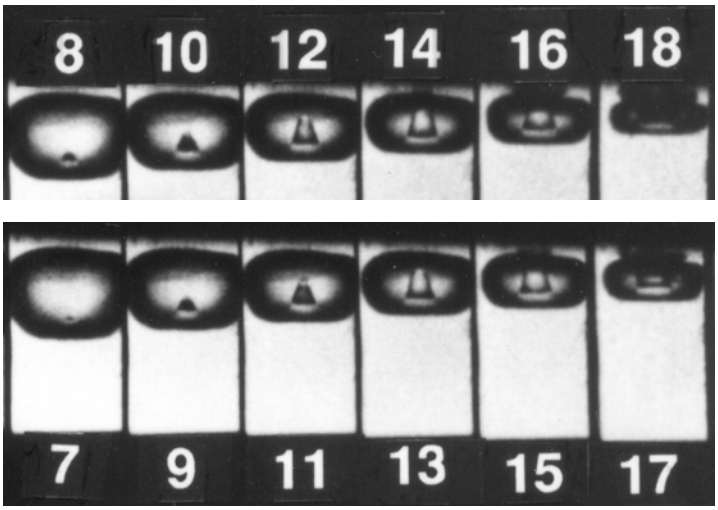

Figure 5.2. Series of photographs showing the development of the microjet in a bubble collapsing very close to a solid wall (at top of frame). The interval between the numbered frames is $2\mu s$ and the frame width is $1.4mm$. From Tomita and Shima (1990), reproduced with permission of the authors.

phase at the end of the collapse when compression of the bubble contents causes d^2R/dt^2 to switch from the small negative values of early collapse to very large positive values when the bubble is close to its minimum size.

This strong instability during the rebound phase appears to have several different consequences. When the bubble surroundings are strongly asymmetrical, for example the bubble is close to a solid wall or a free surface, the dominant perturbation that develops is a re-entrant jet. Of particular interest for cavitation damage is the fact that a nearby solid boundary can cause a re-entrant microjet directed toward that boundary. The surface of the bubble furthest from the wall accelerates inward more rapidly than the side close to the wall and this results in a high-speed re-entrant microjet that penetrates the bubble and can achieve very high speeds. Such microjets were first observed experimentally by Naude and Ellis (1961) and Benjamin and Ellis (1966). The series of photographs shown in figure 5.2 represent a good example of the experimental observations of a developing re-entrant jet. Figure 5.3 presents a comparison between the re-entrant jet development in a bubble collapsing near a solid wall as observed by Lauterborn and Bolle (1975) and as computed by Plesset and Chapman (1971). Note also that depth charges rely for their destructive power on a re-entrant jet directed toward the submarine upon the collapse of the explosively generated bubble.

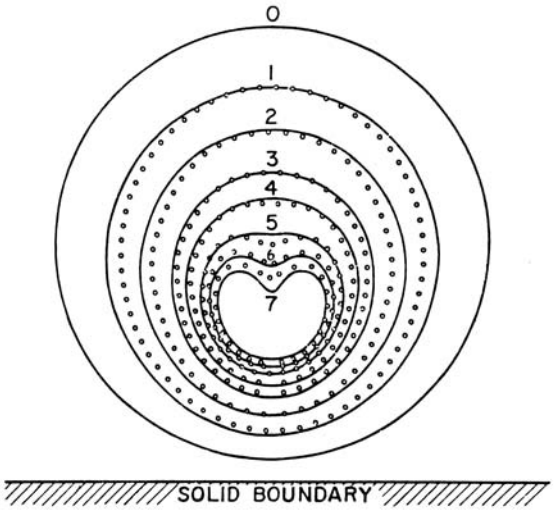

Figure 5.3. The collapse of a cavitation bubble close to a solid boundary in a quiescent liquid. The theoretical shapes of Plesset and Chapman (1971) (solid lines) are compared with the experimental observations of Lauterborn and Bolle (1975) (points). Figure adapted from Plesset and Prosperetti (1977).

Other strong asymmetries can also cause the formation of a re-entrant jet. A bubble collapsing near a free surface produces a re-entrant jet directed *away* from the free surface (Chahine 1977). Indeed, there exists a critical flexibility for a nearby surface that separates the circumstances in which the re-entrant jet is directed away from rather than toward the surface. Gibson and Blake (1982) demonstrated this experimentally and analytically and suggested flexible coatings or liners as a means of avoiding cavitation damage. Another possible asymmetry is the proximity of other, neighboring bubbles in a finite cloud of bubbles. Chahine and Duraiswami (1992) showed that the bubbles on the outer edge of such a cloud will tend to develop jets directed toward the center of the cloud.

When there is no strong asymmetry, the analysis of the Rayleigh-Taylor instability shows that the most unstable mode of shape distortion can be a much higher-order mode. These higher order modes can dominate when a vapor bubble collapses far from boundaries. Thus observations of collapsing cavitation bubbles, while they may show a single vapor/gas volume prior to collapse, just after minimum size the *bubble* appears as a cloud of much smaller bubbles. An example of this is shown in figure 5.4. Brennen (1995) shows how the most unstable mode depends on two parameters representing

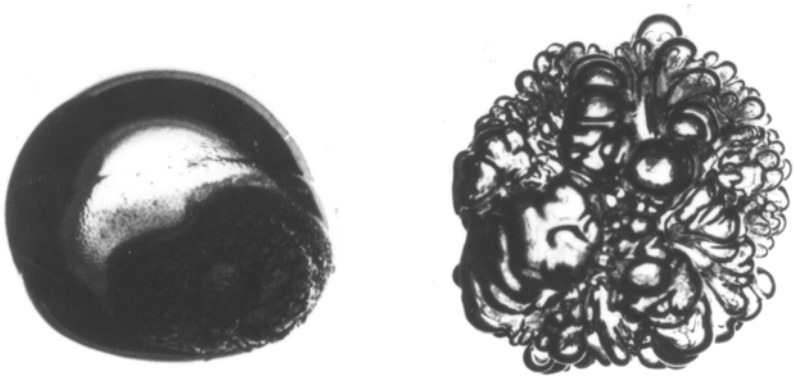

Figure 5.4. Photographs of an ether bubble in glycerine before (left) and after (right) a collapse and rebound, both bubbles being about $5 - 6mm$ across. Reproduced from Frost and Sturtevant (1986) with the permission of the authors.

the effects of surface tension and non-condensable gas in the bubble. That most unstable mode number was later used in one of several analyses seeking to predict the number of fission fragments produced during collapse of a cavitating bubble (Brennen 2002).

5.2.4 Cavitation damage

Perhaps the most ubiquitous engineering problem caused by cavitation is the material damage that cavitation bubbles can cause when they collapse in the vicinity of a solid surface. Consequently, this subject has been studied quite intensively for many years (see, for example, ASTM 1967; Thiruvengadam 1967, 1974; Knapp, Daily, and Hammitt 1970). The problem is a difficult one because it involves complicated unsteady flow phenomena combined with the reaction of the particular material of which the solid surface is made. Though there exist many empirical rules designed to help the engineer evaluate the potential cavitation damage rate in a given application, there remain a number of basic questions regarding the fundamental mechanisms involved. Cavitation bubble collapse is a violent process that generates highly localized, large-amplitude shock waves (section 5.2.2) and microjets (section 5.2.3). When this collapse occurs close to a solid surface, these intense disturbances generate highly localized and transient surface stresses. With softer material, individual pits caused by a single bubble collapse are often observed. But with the harder materials used in most applications it is the repetition of the loading due to repeated collapses that causes local

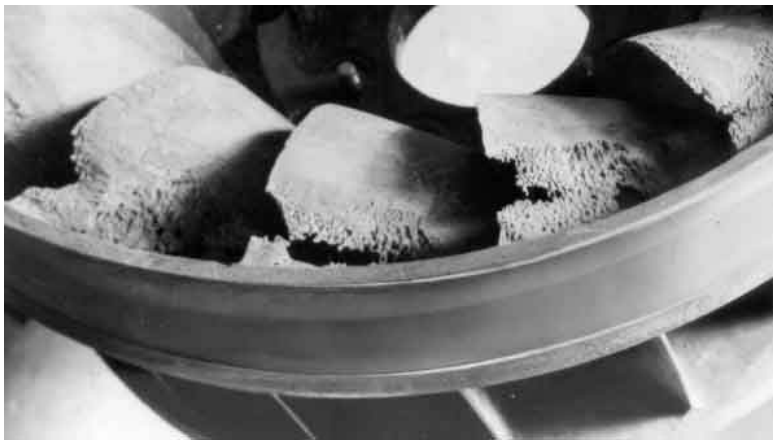

Figure 5.5. Major cavitation damage to the blades at the discharge from a Francis turbine.

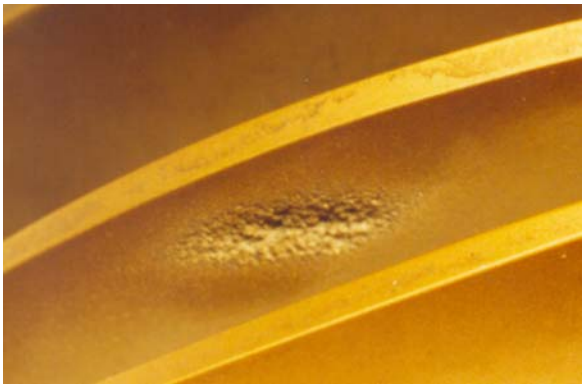

Figure 5.6. Photograph of localized cavitation damage on the blade of a mixed flow pump impeller made from an aluminum-based alloy.

surface fatigue failure and the subsequent detachment of pieces of material. Thus cavitation damage to metals usually has the crystalline appearance of fatigue failure. The damaged runner and pump impeller in figures 5.5 and 5.6 are typical examples

The issue of whether cavitation damage is caused by microjets or by shock waves generated when the remnant cloud of bubble reaches its minimum volume (or by both) has been debated for many years. In the 1940s and 1950s the focus was on the shock waves generated by spherical bubble collapse. When the phenomenon of the microjet was first observed, the focus shifted to studies of the impulsive pressures generated by microjets. First Shima *et al.* (1983) used high speed Schlieren photography to show that a spherical

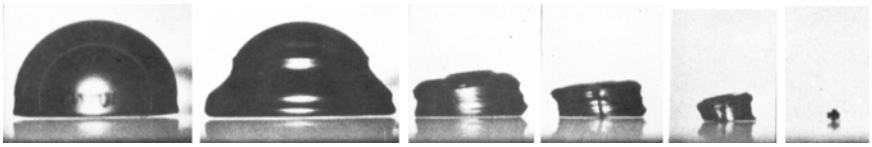

Figure 5.7. Series of photographs of a hemispherical bubble collapsing against a wall showing the *pancaking* mode of collapse. From Benjamin and Ellis (1966) reproduced with permission of the first author.

shock wave was indeed generated by the remnant cloud at the instant of minimum volume. About the same time, Fujikawa and Akamatsu (1980) used a photoelastic material so that they could simultaneously observe the stresses in the solid and measure the acoustic pulses and were able to confirm that the impulsive stresses in the material were initiated at the same moment as the acoustic pulse. They also concluded that this corresponded to the instant of minimum volume and that the waves were not produced by the microjet. Later, however, Kimoto (1987) observed stress pulses that resulted both from microjet impingement and from the remnant cloud collapse shock.

The microjet phenomenon in a quiescent fluid has been extensively studied analytically as well as experimentally. Plesset and Chapman (1971) numerically calculated the distortion of an initially spherical bubble as it collapsed close to a solid boundary and, as figure 5.3 demonstrates, their profiles are in good agreement with the experimental observations of Lauterborn and Bolle (1975). Blake and Gibson (1987) review the current state of knowledge, particularly the analytical methods for solving for bubbles collapsing near a solid or a flexible surface.

It must also be noted that there are many circumstances in which it is difficult to discern a microjet. Some modes of bubble collapse near a wall involve a *pancaking* mode exemplified by the photographs in figure 5.7 and in which no microjet is easily recognized.

Finally, it is important to emphasize that virtually all of the observations described above pertain to bubble collapse in an otherwise quiescent fluid. A bubble that grows and collapses in a flow is subject to other deformations that can significantly alter its collapse dynamics, modify or eliminate the microjet and alter the noise and damage potential of the collapse process. In the next section some of these flow deformations will be illustrated.

5.3 CAVITATION BUBBLES

5.3.1 Observations of cavitating bubbles

We end our brief survey of the dynamics of cavitating bubbles with some experimental observations of single bubbles (single cavitation *events*) in real flows for these reveal the complexity of the micro-fluid-mechanics of individual bubbles. The focus here is on individual events springing from a single nucleus. The interactions between bubbles at higher nuclei concentrations will be discussed later.

Pioneering observations of individual cavitation events were made by Knapp and his associates at the California Institute of Technology in the 1940s (see, for example, Knapp and Hollander 1948) using high-speed movie cameras capable of 20,000 frames per second. Shortly thereafter Plesset (1949), Parkin (1952), and others began to model these observations of the growth and collapse of traveling cavitation bubbles using modifications of Rayleigh's original equation of motion for a spherical bubble. However, observations of real flows demonstrate that even single cavitation bubbles are often highly distorted by the pressure gradients in the flow. Before describing some of the observations, it is valuable to consider the relative sizes of the cavitation bubbles and the viscous boundary layer. In the flow of a uniform stream of velocity, U, around an object such as a hydrofoil with typical dimension, ℓ, the thickness of the laminar boundary layer near the minimum pressure point will be given qualitatively by $\delta = (\nu_L \ell/U)^{\frac{1}{2}}$. Comparing this with the typical maximum bubble radius, R_m, given by equation 5.4, it follows that the ratio, δ/R_m, is roughly given by

$$\frac{\delta}{R_m} = \frac{1}{2(-\sigma - C_{pmin})} \left\{ \frac{\nu_L}{\ell U} \right\}^{\frac{1}{2}} \tag{5.6}$$

Therefore, provided $(-\sigma - C_{pmin})$ is of the order of 0.1 or greater, it follows that for the high Reynolds numbers, $U\ell/\nu_L$, that are typical of most of the flows in which cavitation is a problem, the boundary layer is usually much thinner than the typical dimension of the bubble.

Recently, Ceccio and Brennen (1991) and Kuhn de Chizelle *et al.* (1992a,b) have made an extended series of observations of cavitation bubbles in the flow around axisymmetric bodies, including studies of the scaling of the phenomena. The observations at lower Reynolds numbers are exemplified by the photographs of bubble profiles in figure 5.8. In all cases the shape during the initial growth phase is that of a spherical cap, the bubble being separated from the wall by a thin layer of liquid of the same order of magnitude as the boundary layer thickness. Later developments depend on the geometry

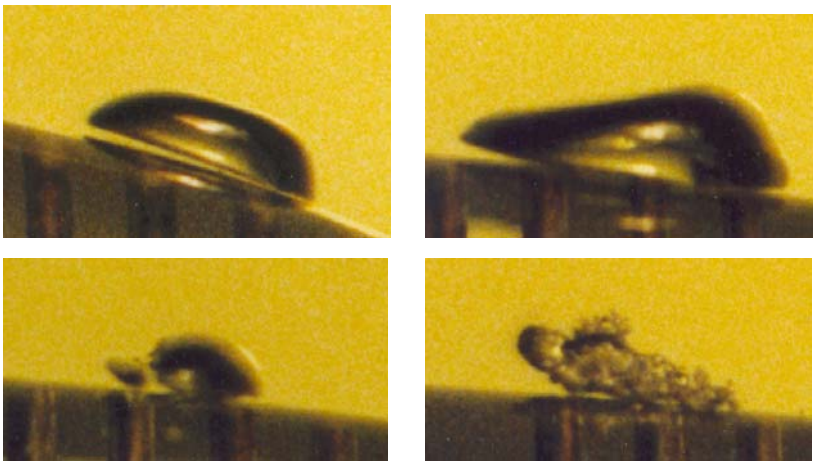

Figure 5.8. A series of photographs illustrating, in profile, the growth and collapse of a traveling cavitation bubble in a flow around a $5.08cm$ diameter headform at $\sigma = 0.45$ and a speed of 9 m/s. the sequence is top left, top right, bottom left, bottom right, the flow is from right to left. The lifesize width of each photograph is $0.73cm$. From Ceccio and Brennen (1991).

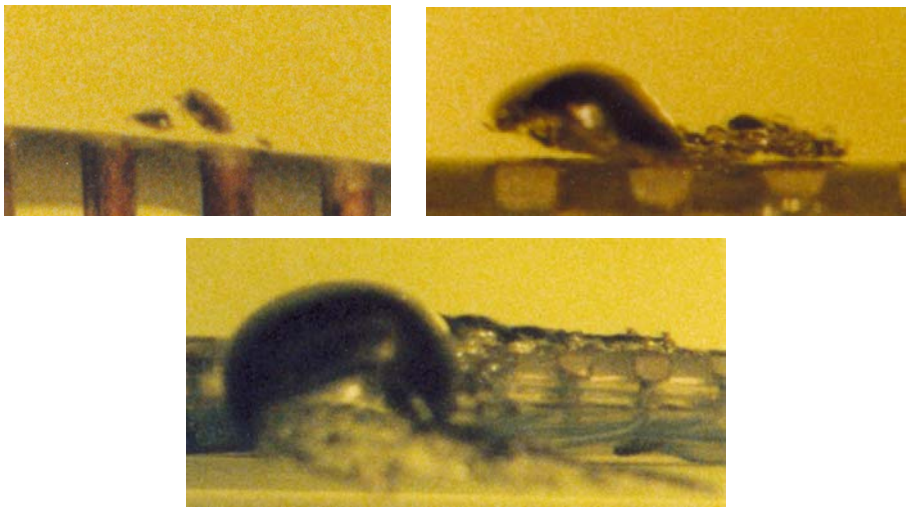

Figure 5.9. Examples of bubble fission (upper left), the instability of the liquid layer under a traveling cavitation bubble (upper right) and the attached tails (lower). From Ceccio and Brennen (1991) experiments with a $5.08cm$ diameter ITTC headform at $\sigma = 0.45$ and a speed of $8.7m/s$. The flow is from right to left. The lifesize widths of the photographs are $0.63cm$, $0.80cm$ and $1.64cm$ respectively.

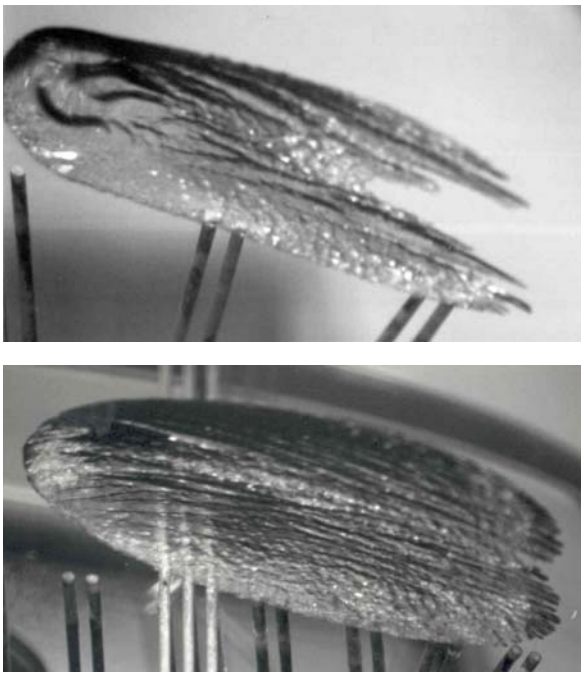

Figure 5.10. Typical cavitation events from the scaling experiments of Kuhn de Chizelle *et al.* (1992b) showing transient bubble-induced patches, the upper one occurring on a 50.8 cm diameter Schiebe headform at $\sigma = 0.605$ and a speed of 15 m/s, the lower one on a 25.4 cm headform at $\sigma = 0.53$ and a speed of 15 m/s. The flow is from right to left. The lifesize widths of the photographs are 6.3cm (top) and 7.6cm (bottom).

of the headform and the Reynolds number. In some cases as the bubble enters the region of adverse pressure gradient, the exterior frontal surface is pushed inward, causing the profile of the bubble to appear wedge-like. Thus the collapse is initiated on the exterior frontal surface of the bubble, and this often leads to the bubble fissioning into forward and aft bubbles as seen in figure 5.8. At the same time, the bubble acquires significant spanwise vorticity through its interactions with the boundary layer during the growth phase. Consequently, as the collapse proceeds, this vorticity is concentrated and the bubble evolves into one (or two or possibly more) short cavitating vortices with spanwise axes. These vortex bubbles proceed to collapse and seem to rebound as a cloud of much smaller bubbles. Ceccio and Brennen (1991) (see also Kumar and Brennen 1993) conclude that the flow-induced fission prior to collapse can have a substantial effect on the noise produced.

Two additional phenomena were observed. In some cases the layer of liquid underneath the bubble would become disrupted by some instability, creating

a bubbly layer of fluid that subsequently gets left behind the main bubble (see figure 5.9). Second, it sometimes happened that when a bubble passed a point of laminar separation, it triggered the formation of local *attached cavitation* streaks at the lateral or spanwise extremities of the bubble, as seen in figure 5.9. Then, as the main bubble proceeds downstream, these *streaks* or *tails* of attached cavitation are stretched out behind the main bubble, the trailing ends of the tails being attached to the solid surface. Tests at much higher Reynolds numbers (Kuhn de Chizelle *et al.* 1992a,b) revealed that these *events with tails* occured more frequently and would initiate attached cavities over the entire wake of the bubble as seen in figure 5.10. Moreover, the attached cavitation would tend to remain for a longer period after the main bubble had disappeared. Eventually, at the highest Reynolds numbers tested, it appeared that the passage of a single bubble was sufficient to trigger a *patch* of attached cavitation (figure 5.10, bottom), that would persist for an extended period after the bubble had long disappeared.

In summary, cavitation bubbles are substantially deformed and their dynamics and acoustics altered by the flow fields in which they occur. This necessarily changes the noise and damage produced by those cavitation events.

5.3.2 Cavitation noise

The violent and catastrophic collapse of cavitation bubbles results in the production of noise that is a consequence of the momentary large pressures that are generated when the contents of the bubble are highly compressed. Consider the flow in the liquid caused by the volume displacement of a growing or collapsing cavity. In the far field the flow will approach that of a simple source, and it is clear that equation 4.5 for the pressure will be dominated by the first term on the right-hand side (the unsteady inertial term) since it decays more slowly with radius, r, than the second term. If we denote the time-varying volume of the cavity by $V(t)$ and substitute using equation 4.2, it follows that the time-varying component of the pressure in the far field is given by

$$p_a = \frac{\rho_L}{4\pi\mathcal{R}} \frac{d^2V}{dt^2} \tag{5.7}$$

where p_a is the radiated acoustic pressure and we denote the distance, r, from the cavity center to the point of measurement by $\mathcal{R}$ (for a more thorough treatment see Dowling and Ffowcs Williams 1983 and Blake 1986b). Since the noise is directly proportional to the second derivative of the volume with

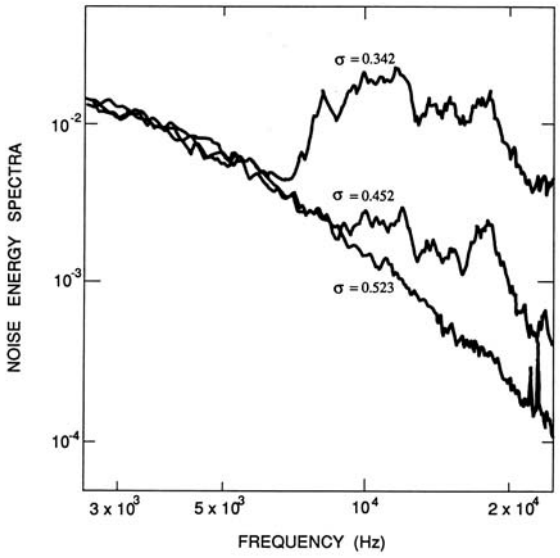

Figure 5.11. Acoustic power spectra from a model spool valve operating under noncavitating ($\sigma = 0.523$) and cavitating ($\sigma = 0.452$ and 0.342) conditions (from the investigation of Martin *et al.* 1981).

respect to time, it is clear that the noise pulse generated at bubble collapse occurs because of the very large and positive values of d^2V/dt^2 when the bubble is close to its minimum size. It is conventional (see, for example, Blake 1986b) to present the sound level using a root mean square pressure or *acoustic* pressure, p_s, defined by

$$p_s^2 = \overline{p_a^2} = \int_0^\infty \mathcal{G}(f)df \tag{5.8}$$

and to represent the distribution over the frequency range, f, by the spectral density function, $\mathcal{G}(f)$.

To the researcher or engineer, the crackling noise that accompanies cavitation is one of the most evident characteristics of the phenomenon. The onset of cavitation is often detected first by this noise rather than by visual observation of the bubbles. Moreover, for the practical engineer it is often the primary means of detecting cavitation in devices such as pumps and valves. Indeed, several empirical methods have been suggested that estimate the rate of material damage by measuring the noise generated (for example, Lush and Angell 1984).

The noise due to cavitation in the orifice of a hydraulic control valve is typical, and spectra from such an experiment are presented in figure 5.11.

The lowest curve at $\sigma = 0.523$ represents the turbulent noise from the noncavitating flow. Below the incipient cavitation number (about 0.523 in this case) there is a dramatic increase in the noise level at frequencies of about $5kHz$ and above. The spectral peak between $5kHz$ and $10kHz$ corresponds closely to the expected natural frequencies of the nuclei present in the flow (see section 4.4.1).

Most of the analytical approaches to cavitation noise build on knowledge of the dynamics of collapse of a single bubble. Fourier analyses of the radiated acoustic pressure due to a single bubble were first visualized by Rayleigh (1917) and implemented by Mellen (1954) and Fitzpatrick and Strasberg (1956). In considering such Fourier analyses, it is convenient to nondimensionalize the frequency by the typical time span of the whole event or, equivalently, by the collapse time, t_{tc}, given by equation 4.36. Now consider the frequency content of $\mathcal{G}(f)$ using the dimensionless frequency, ft_{tc}. Since the volume of the bubble increases from zero to a finite value and then returns to zero, it follows that for $ft_{tc} < 1$ the Fourier transform of the volume is independent of frequency. Consequently d^2V/dt^2 will be proportional to f^2 and therefore $\mathcal{G}(f) \propto f^4$ (see Fitzpatrick and Strasberg 1956). This is the origin of the left-hand asymptote in figure 5.12.

The behavior at intermediate frequencies for which $ft_{tc} > 1$ has been the subject of more speculation and debate. Mellen (1954) and others considered the typical equations governing the collapse of a spherical bubble in the absence of thermal effects and noncondensable gas (equation 4.32) and concluded that, since the velocity $dR/dt \propto R^{-\frac{3}{2}}$, it follows that $R \propto t^{\frac{2}{5}}$. Therefore the Fourier transform of d^2V/dt^2 leads to the asymptotic behavior $\mathcal{G}(f) \propto f^{-\frac{2}{5}}$. The error in this analysis is the neglect of the noncondensable gas. When this is included and when the collapse is sufficiently advanced, the last term in the square brackets of equation 4.32 becomes comparable with the previous terms. Then the behavior is quite different from $R \propto t^{\frac{2}{5}}$. Moreover, the values of d^2V/dt^2 are much larger during this rebound phase, and therefore the frequency content of the rebound phase will dominate the spectrum. It is therefore not surprising that the $f^{-\frac{2}{5}}$ is not observed in practice. Rather, most of the experimental results seem to exhibit an intermediate frequency behavior like f^{-1} or f^{-2}. Jorgensen (1961) measured the noise from submerged, cavitating jets and found a behavior like f^{-2} at the higher frequencies (see figure 5.12). However, most of the experimental data for cavitating bodies or hydrofoils exhibit a weaker decay. The data by Arakeri and Shangumanathan (1985) from cavitating headform experiments

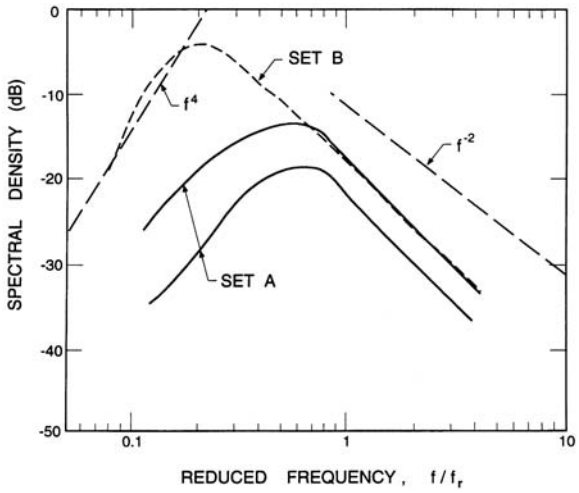

Figure 5.12. Acoustic power spectra of the noise from a cavitating jet. Shown are mean lines through two sets of data constructed by Blake and Sevik (1982) from the data by Jorgensen (1961). Typical asymptotic behaviors are also indicated. The reference frequency, f_r, is $(p_\infty/\rho_L d^2)^{\frac{1}{2}}$ where d is the jet diameter.

show a very consistent f^{-1} trend over almost the entire frequency range, and very similar results have been obtained by Ceccio and Brennen (1991).

Ceccio and Brennen (1991) recorded the noise from individual cavitation bubbles in a flow; a typical acoustic signal from their experiments is reproduced in figure 5.13. The large positive pulse at about 450 μs corresponds to the first collapse of the bubble. This first pulse in figure 5.13 is followed by some facility-dependent oscillations and by a second pulse at about 1100 μs. This corresponds to the second collapse that follows the rebound from the first collapse.

A good measure of the magnitude of the collapse pulse is the acoustic impulse, I, defined as the area under the pulse or

$$I = \int_{t_1}^{t_2} p_a dt \tag{5.9}$$

where t_1 and t_2 are times before and after the pulse at which p_a is zero. For later purposes we also define a dimensionless impulse, I^*, as

$$I^* = 4\pi I \mathcal{R}/\rho_L U \ell^2 \tag{5.10}$$

where U and ℓ are the reference velocity and length in the flow. The average acoustic impulses for individual bubble collapses on two axisymmetric

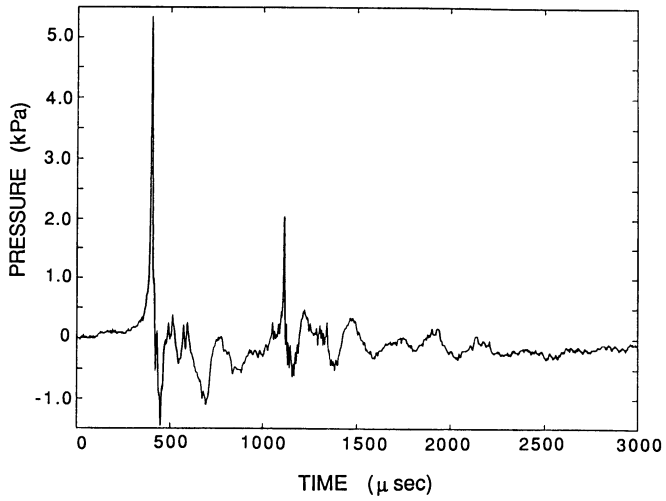

Figure 5.13. A typical acoustic signal from a single collapsing bubble. From Ceccio and Brennen (1991).

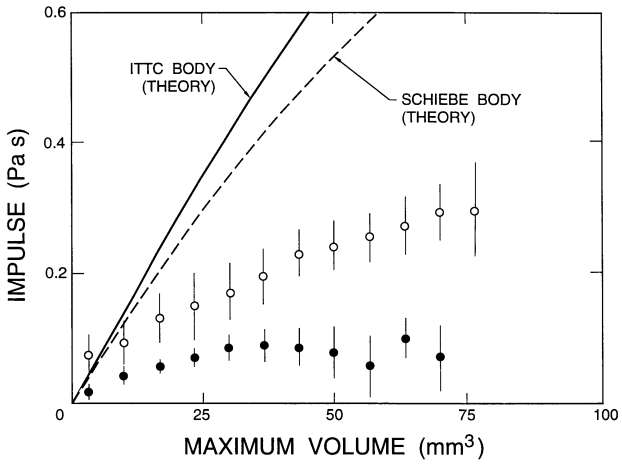

Figure 5.14. Comparison of the acoustic impulse, I, produced by the collapse of a single cavitation bubble on two axisymmetric headforms as a function of the maximum volume prior to collapse. Open symbols: average data for Schiebe headform; closed symbols: ITTC headform; vertical lines indicate one standard deviation. Also shown are the corresponding results from the solution of the Rayleigh-Plesset equation. From Ceccio and Brennen (1991).

headforms (ITTC and Schiebe headforms) are compared in figure 5.14 with impulses predicted from integration of the Rayleigh-Plesset equation. Since these theoretical calculations assume that the bubble remains spherical, the discrepancy between the theory and the experiments is not too surprising. Indeed one interpretation of figure 5.14 is that the theory can provide an order of magnitude estimate and an upper bound on the noise produced by a single bubble. In actuality, the departure from sphericity produces a less focused collapse and therefore less noise.

The next step is to consider the synthesis of cavitation noise from the noise produced by individual cavitation bubbles or events. If the impulse produced by each event is denoted by I and the number of events per unit time is denoted by $\dot{n}$, the sound pressure level, p_s, will be given by

$$p_s = I\dot{n} \tag{5.11}$$

Consider the scaling of cavitation noise that is implicit in this construct. Both the experimental results and the analysis based on the Rayleigh-Plesset equation indicate that the nondimensional impulse produced by a single cavitation event is strongly correlated with the maximum volume of the bubble prior to collapse and is almost independent of the other flow parameters. It follows from equations 5.7 and 5.9 that

$$I^* = \frac{1}{U\ell^2}\left\{\left(\frac{dV}{dt}\right)_{t_2} - \left(\frac{dV}{dt}\right)_{t_1}\right\} \tag{5.12}$$

and the values of dV/dt at the moments $t = t_1, t_2$ when $d^2V/dt^2 = 0$ may be obtained from the Rayleigh-Plesset equation. If the bubble radius at the time t_1 is denoted by R_x and the coefficient of pressure in the liquid at that moment is denoted by C_{px}, then

$$I^* \approx 8\pi\left(\frac{R_x}{\ell}\right)^2 (C_{px} - \sigma)^{\frac{1}{2}} \tag{5.13}$$

Numerical integrations of the Rayleigh-Plesset equation for a range of typical circumstances yield $R_x/R_m \approx 0.62$ where R_m is the maximum volumetric radius and that $(C_{px} - \sigma) \propto R_m/\ell$ (in these calculations ℓ was the headform radius) so that

$$I^* \approx \beta\left(\frac{R_m}{\ell}\right)^{\frac{5}{2}} \tag{5.14}$$

The aforementioned integrations of the Rayleigh-Plesset equation yield a factor of proportionality, β, of about 35. Moreover, the upper envelope of

the experimental data of which figure 5.14 is a sample appears to correspond to a value of $\beta \approx 4$. We note that a quite similar relation between I^* and R_m/ℓ emerges from the analysis by Esipov and Naugol'nykh (1973) of the compressive sound wave generated by the collapse of a gas bubble in a compressible liquid.

From the above relations, it follows that

$$I \approx \frac{\beta}{12}\rho_L U R_m^{\frac{5}{2}}/\mathcal{R}\ell^{\frac{1}{2}} \tag{5.15}$$

Consequently, the evaluation of the impulse from a single event is completed by an estimate of R_m such as that of equation 5.4. Since that estimate has R_m independent of U for a given cavitation number, it follows that I is linear with U.

The event rate, $\dot{n}$, can be considerably more complicated to evaluate than might at first be thought. If all the nuclei flowing through a certain, known streamtube (say with a cross-sectional area, A_n, in the upstream flow) were to cavitate similarly, then the result would be

$$\dot{n} = nA_nU \tag{5.16}$$

where n is the nuclei concentration (number/unit volume) in the incoming flow. Then it follows that the acoustic pressure level resulting from substituting equations 5.16, 5.15 into equation 5.11 and using equation 5.4 becomes

$$p_s \approx \frac{\beta}{3}\rho_L U^2 A_n n\ell^2(-\sigma - C_{pmin})^{\frac{5}{2}}/\mathcal{R} \tag{5.17}$$

where we have omitted some of the constants of order unity. For the relatively simple flows considered here, equation 5.17 yields a sound pressure level that scales with U^2 and with ℓ^4 because $A_n \propto \ell^2$. This scaling with velocity does correspond roughly to that which has been observed in some experiments on traveling bubble cavitation, for example, those of Blake, Wolpert, and Geib (1977) and Arakeri and Shangumanathan (1985). The former observe that $p_s \propto U^m$ where $m = 1.5$ to 2.

Different scaling laws will apply when the cavitation is generated by turbulent fluctuations such as in a turbulent jet (see, for example, Ooi 1985 and Franklin and McMillan 1984). Then the typical tension experienced by a nucleus as it moves along a disturbed path in a turbulent flow is very much more difficult to estimate. Consequently, the models for the sound pressure due to cavitation in a turbulent flow and the scaling of that sound with velocity are less well understood.

5.3.3 Cavitation luminescence

Though highly localized both temporally and spatially, the extremely high temperatures and pressures that can occur in the noncondensable gas during collapse are believed to be responsible for the phenomenon known as luminescence, the emission of light that is observed during cavitation bubble collapse. The phenomenon was first observed by Marinesco and Trillat (1933), and a number of different explanations were advanced to explain the emissions. The fact that the light was being emitted at collapse was first demonstrated by Meyer and Kuttruff (1959). They observed cavitation on the face of a rod oscillating magnetostrictively and correlated the light with the collapse point in the growth-and-collapse cycle. The balance of evidence now seems to confirm the suggestion by Noltingk and Neppiras (1950) that the phenomenon is caused by the compression and adiabatic heating of the noncondensable gas in the collapsing bubble. As we discussed previously in sections 4.2.4 and 5.2.2, temperatures of the order of $6000°K$ can be anticipated on the basis of uniform compression of the noncondensable gas; the same calculations suggest that these high temperatures will last for only a fraction of a microsecond. Such conditions would explain the emission of light. Indeed, the measurements of the spectrum of sonoluminescence by Taylor and Jarman (1970), Flint and Suslick (1991), and others suggest a temperature of about $5000°K$. However, some recent experiments by Barber and Putterman (1991) indicate much higher temperatures and even shorter emission durations of the order of picoseconds. Speculations on the explanation for these observations have centered on the suggestion by Jarman (1960) that the collapsing bubble forms a spherical, inward-propagating shock in the gas contents of the bubble and that the focusing of the shock at the center of the bubble is an important reason for the extremely high apparent *temperatures* associated with the sonoluminescence radiation. It is, however, important to observe that spherical symmetry is essential for this mechanism to have any significant consequences. One would therefore expect that the distortions caused by a flow would not allow significant shock focusing and would even reduce the effectiveness of the basic compression mechanism.